Article

Quantitative Determination of the Complex Polarizability of Individual Nanoparticles by Scanning Cavity Microscopy

Matthias Mader,* Julia Benedikter, Lukas Husel, Theodor W. Hänsch, and David Hunger*

Cite This: *ACS Photonics* 2022, 9, 466–473

Read Online

ACCESS | Metrics & More | Article Recommendations | Supporting Information

ABSTRACT: The complex polarizability describes the complete optical properties of a nanoobject in the Rayleigh limit, including its absorption, scattering, and dispersion. A large range of applications would benefit from the capability to infer the polarizability on a single-particle level; however, it requires two complementary measurements to fully determine this quantity, and the smallness of the signals makes this highly challenging. Here we use signal enhancement in a tunable high finesse fiber cavity and apply noise-rejecting differential measurement techniques to simultaneously obtain the extinction cross section and the dispersion of individual gold nanospheres, which allows us to quantitatively obtain the real and imaginary part of the polarizability with high precision. We achieve a detection limit for extinction cross sections of 1.8 nm^2 and for the polarizability of $\alpha/\epsilon_0 = (28\,000 + 200i)$ nm^3. Our method opens the way to a full characterization of the optical properties of individual nanosystems, with applications ranging from nanomaterial science to biology.

**KEYWORDS:** *nanoparticles, polarizability, extinction, microscopy, microcavity*

ptical characterization of individual nanosystems provides insight into their physical, chemical, and biological properties. To optimize absorption and scattering properties of nanomaterials for specific applications, such as photovoltaics,[1] labeling,[2] or displays,[3] the quantitative knowledge of absorption and scattering cross sections is crucial. For spherical particles in the Rayleigh limit with a size much smaller than the wavelength, the two cross sections are directly related to the complex polarizability, and this quantity fully describes their optical properties.[4−6] To achieve the required high sensitivity for single-particle measurements on nanomaterials, sophisticated techniques such as spatial modulation spectroscopy,[7] photothermal imaging,[8] interferometric scattering,[9] and scanning near-field microscopy[10,11] have been developed. So far, the above techniques cannot measure both absorption and scattering independently, and extraction of quantitative values has been shown only for a few cases.[12,13] Recently, correlative transmission and scattering microscopy was used to demonstrate the quantitative measurement of scattering and absorption cross sections by combining dark and bright field microscopy. However, the technique requires precise knowledge of the experimental illumination, sample, substrate, and collection geometry[14,15] and has been limited to a sensitivity for cross sections of ~500 nm^2. In a comprehensive way, spectrally resolved quantitative determination of the complex polarizability was recently demonstrated for both plasmonic and dielectric nanoparticles, however, also limited to rather large cross sections ≫1 × 10^3 nm^2.[16] One of the earliest and
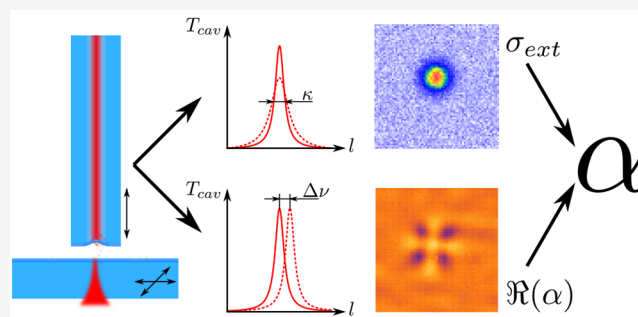
extremely sensitive measurements of the complex dielectric constant of single gold nanoparticles used differential interference contrast.[17]

To cope with the extremely small signals, significant efforts in reducing noise by averaging, noise rejection, and signal processing are commonly used. In a different approach, optical microcavities can provide substantial signal enhancement by recirculating the probe light for multiple interactions with the sample. Monolithic whispering gallery mode resonators achieve the highest sensitivity for dispersion and extinction of samples.[18,19] Using photothermal transduction, absorption cross sections can also be measured separately.[20] However, the uncontrolled overlap between the sample and the cavity mode generally hinders quantitative measurements. Alternatively, tunable open access microcavities[21−25] allow one to combine cavity enhancement with microscopy to fully map samples with a so-called scanning cavity microscope (SCM) and have been shown to achieve the highest sensitivity for quantitative measurements of the extinction cross section and near-diffraction limited spatial resolution.[26−28] In SCM, due to
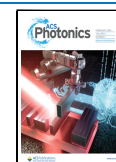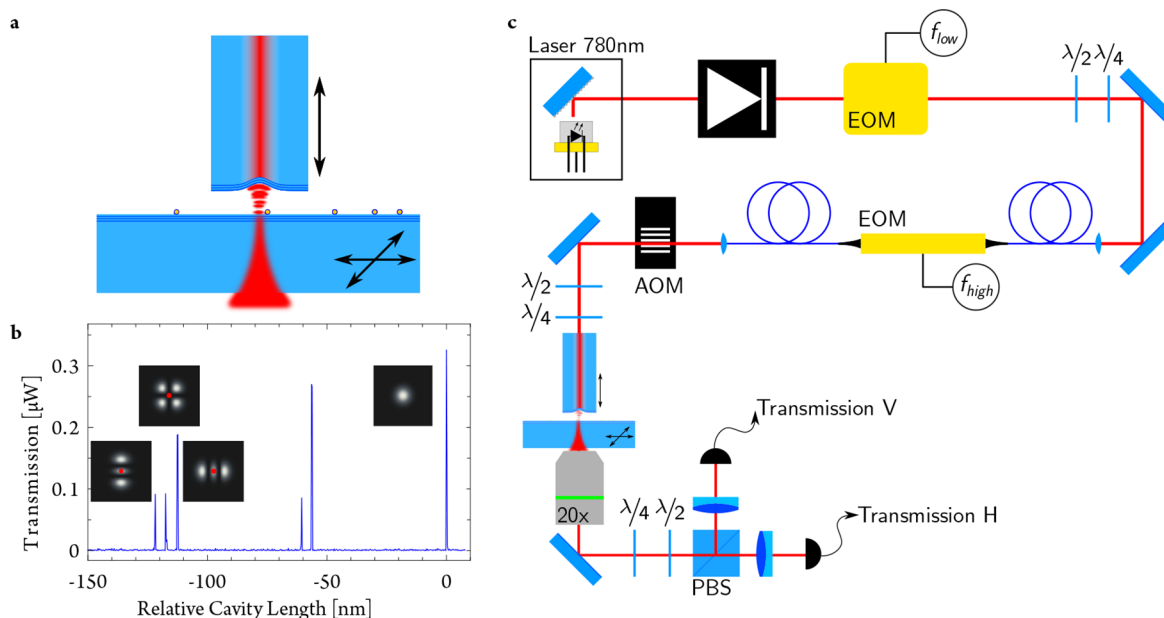
Figure 1. (a) Schematic setup showing the cavity with the laser-machined micromirror at the end-facet of a fiber and a macroscopic plane mirror carrying the gold particles. (b) Cavity transmission signal when changing the mirror separation. The fundamental TEM$_{00}$ mode is used to evaluate the extinction (mode profile as inset on the very right), while the frequency differences of the TEM$_{02}$, TEM$_{11}$, and TEM$_{20}$ modes (mode profiles shown (from left to right) in the insets together with a nanoparticle in the center (red dot)) are used to evaluate differential dispersive frequency shifts. (c) Optical setup, including a probe laser at 780 nm, and two EOMs for high-frequency and low-frequency modulations.

the large tunability of the cavity, the determination of small frequency shifts is challenging and has been demonstrated only for low-finesse cavities,[27] or in a differential manner to resolve birefringence,[26] which however does not give information about the absolute value of the polarizability. Alternatively, within a microfluidic environment, measurements of the real part of the polarizability and the extinction cross section have been demonstrated in an open microcavity,[29,30] however, without differentiation between scattering and absorption and without imaging capabilites.

Here, we use a SCM based on a fiber-based high-finesse Fabry-Pérot optical microcavity[22] to demonstrate quantitative measurements of the complex polarizability of individual gold nanoparticles with highest sensitivity. We simultaneously measure the extinction signal by quantifying the intracavity loss introduced by the sample and measure the real part of the polarizability by observing dispersive frequency shifts of the cavity resonance frequency. The challenge for the latter measurement is to separate frequency shifts due to the sample, which correspond to cavity length changes on a picometer level, from mechanical noise of the widely scannable cavity setup, which shows typical amplitudes on a nanometer-level.

To overcome these mechanical limitations, we demonstrate a differential measurement scheme exploiting relative frequency shifts of higher order transverse modes that are differently affected by a nanoparticle inside the cavity. Without the need of sophisticated cavity stabilization or vibration isolation, we are able to resolve frequency shifts below one cavity line width, while imaging surfaces as large as 100 μm × 100 μm.

We show spatially resolved simultaneous measurements of the extinction and dispersion of individual 50 nm gold nanoparticles and use it to retrieve the real and imaginary part of the polarizability α. We achieve a measurement noise limit of 1.8 nm^2 for the extinction cross section, and 135 MHz

or 0.6 cavity line widths for the dispersive frequency shift, equivalent to a polarizability $\alpha/\epsilon_0 = (28\,000 + 200i)$ nm^3.

■ MEASUREMENT PRINCIPLE

Measuring the complex polarizability α of individual nanoparticles typically requires two independent measurements to determine its real and imaginary part. First, we measure the extinction cross section as the sum of the absorption- and scattering cross section of the particles, in the Rayleigh limit given by

$$\sigma_{\text{ext}} = \sigma_{\text{abs}} + \sigma_{\text{sca}} = \frac{2\pi}{\lambda\epsilon_0}\Im(\alpha) + \left(\frac{2\pi}{\lambda}\right)^4 \frac{1}{6\pi\epsilon_0^2}|\alpha|^2 \tag{1}$$

with the probe wavelength λ, speed of light c, and the vacuum permittivity ϵ_0.[4-6] To infer this quantity, we measure the change of the cavity linewidth due to a particle interacting with the cavity mode having a $1/e^2$ radius w_0. This introduces an additional loss $2L = 8\,\sigma_{\text{ext}}/(\pi w_0^2)$ (see Supporting Information, note 1, for more details), leading to an increase of the resonator linewidth of $\kappa = (2L + L_1 + T_1 + L_2 + T_2)c/(2\,d)$, where d is the optical resonator length including field penetration into the mirror coating and T_i and L_i are the transmission and losses of each mirror, respectively.

In a second step, the real part of the polarizability is measured by observing the dispersive shift of the cavity's resonance frequency,[19,31] which is given by

$$\Delta\nu_{l,m} = \frac{c\Re(\alpha)}{2\epsilon_0\lambda V_m}u_{l,m}^2(x, y, z) \tag{2}$$

where $u_{l,m}(x, y, z)$ is the normalized Hermite-Gaussian cavity mode, with transverse mode index (l, m) at the position of the particle and $V_m = \int|u_{l,m}(r)|^2 d^3r = \pi w_0^2 d/4$ being the mode volume.[32-34]
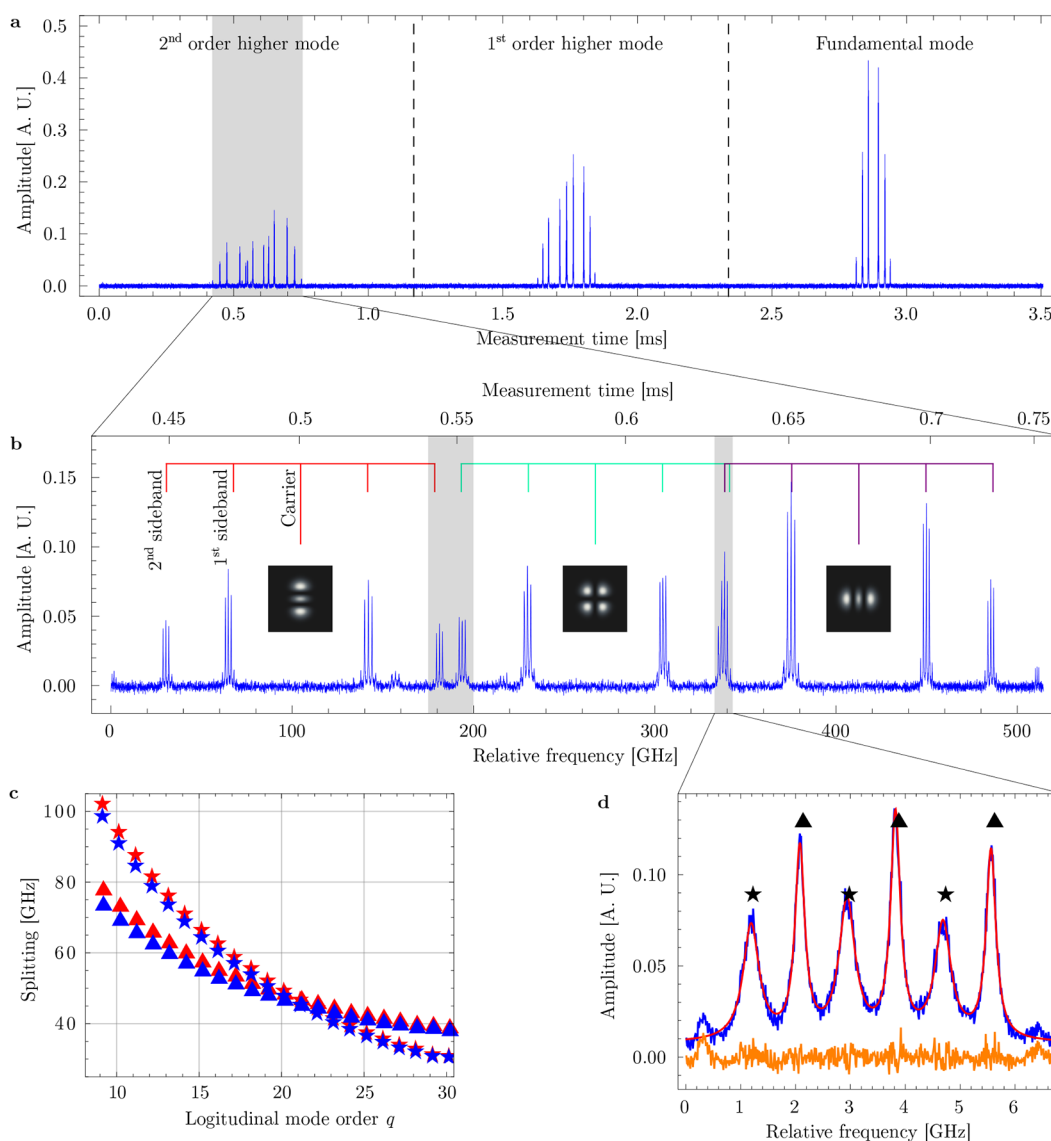
Figure 2. (a) Raw cavity transmission signal spanning the first three transverse mode orders TEM_{00}, TEM_{01}/TEM_{10}, and $TEM_{02}/TEM_{11}/TEM_{20}$ under high- and low-frequency modulations. (b) Zoom into the second higher order mode family. The carriers are fully suppressed, and the high-frequency modulation frequency is chosen such that the second order sidebands of TEM_{02} and TEM_{11}, as well as TEM_{11} and TEM_{20}, have minimal frequency separation. Resonances belonging to the same modes are indicated by colored brackets centered around the position of the resonances of an unmodulated laser; regions of the signal used for further evaluations are shaded gray. (d) Additional low frequency sidebands serve as local frequency markers. A simultaneous fit (red solid line) of the six resonances yields the mode frequency separation, symbols indicate peaks of each order. The residuum (orange) proves the quality of the fit. (c) Mode frequency splitting of the TEM_{02}/TEM_{11} (triangles) and the TEM_{11}/TEM_{20} (stars) modes for both linear polarization modes (blue/red) as a function of the cavity length. Note: this measurement has been performed with the micromirror used to retrieve the presented results. The measurements for (a), (b), and (d) have been done with a different micromirror.

Combining both measurements allows one to retrieve the polarizability α.

The cavity design used in the experiments is depicted schematically in Figure 1a: the resonator consists of a macroscopic plane mirror and a concave micromirror (radius of curvature $r_c = 40~\mu m$) on the end-facet of a single mode optical fiber machined with a CO_2 laser.[22,35] The super-polished plane mirror substrate (fused silica, rms roughness < 0.2 nm) is coated with a Bragg mirror for a center wavelength at 780 nm, designed such that the maximum of the cavity standing wave is slightly above the mirror surface. It has a design transmission of $T_1 = 30$ ppm and a measured combined absorption and scattering loss $L_1 = 14$ ppm. The fiber tip is

coated for the same center wavelength with $T_2 = 16$ ppm and $L_2 = 16$ ppm. At the mirror separation used for the measurements shown here, $d = 8~\mu m$, a cavity built from the two mirrors achieves a measured finesse of $\mathcal{F} = 86800$, consistent with the above numbers.

The sensitivity of the cavity for extinction and dispersion measurements is governed by the cooperativity parameter $C = 3/\pi^2 \cdot \mathcal{F}\lambda^2/(\pi w_0^2)$, which serves as the central figure of merit.[26,33,36] It is evident that high-finesse cavities with small mode cross sections are desired, which is identical to high quality factors and small mode volumes, $\mathcal{F}/w_0^2 \sim Q/V$. In our experiment we achieve state-of-the-art values with $\mathcal{F} = 86800$ and $w_0 = 2.0~\mu m$, leading to $C = 1.3 \times 10^3$. The measurement

signal for extinction, where one compares the empty cavity linewidth κ_0 with κ in the presence of a sample, can be written as $\kappa/\kappa_0 = 1 + 4\pi/(3\lambda^2)\cdot C\sigma_{ext}$, which makes the linear dependence on C explicit. In the same way, the dispersive cavity frequency shift $\Delta\nu$ normalized to the cavity linewidth becomes $\Delta\nu/\kappa_0 = 4\pi^2/(3\epsilon_0\lambda^3)\cdot C\mathfrak{R}(\alpha)$. With C and the other constants known, it is straightforward to quantitatively obtain $\{\sigma_{ext}, \mathfrak{R}(\alpha)\}$ from a quantitative measurement of $\{\kappa/\kappa_0, \Delta\nu/\kappa_0\}$, which only involves frequency measurements that can be highly accurate.

As a reference sample that also allows a calculation of the polarizability for comparison, we choose gold nanoparticles (GNP) with a nominal diameter of 50 nm. Note that we probe at a wavelength that is far detuned from the plasmon resonance, such that the extinction cross section is about 2 orders of magnitude smaller than on resonance and the dispersive shift is comparable to a dielectric nanoparticle of same size. This choice further provides an example of ultrasmall extinction and scattering cross sections with comparable size. At the same time, the particles can still be imaged by dark field scattering microscopy on resonance, such that proper sample preparation can be monitored non-invasively. We spin-coat commercially available GNPs (BBI Solutions, measured diameter (48.5 ± 1.9) nm) on the plane mirror with a low density ($<1 \times 10^{-3}$ GNP/μm^2).

In the experiment, the light of a grating-stabilized diode laser at 780 nm is frequency stabilized, frequency modulated by a high frequency (up to 40 GHz) and a low frequency (1.747 GHz) electro optical modulator (EOM), and coupled into the cavity through the fiber, see Figure 1c. Light transmitted through the plane mirror is detected polarization selectively with two non-counting avalanche photodiodes. We modulate the cavity length to record the resonances of the fundamental TEM_{00} mode and the first two higher order mode families, in particular, the TEM_{02}, TEM_{11}, and TEM_{20} modes, as shown in Figure 2a. To optimally exploit the dynamic range of the photodetectors and the digitizer, the transmitted power of each transverse mode is equalized using an acousto-optic modulator (AOM). A locking laser at 969 nm that probes the cavity at very low finesse is used to keep the cavity length offset constant on a nm scale during the experiment (not shown in Figure 1c). To initially set the resonator length, the broad spectrum of a superluminescent diode is sent through the cavity, and the length is determined by observing the transmitted spectrum with a grating spectrometer.

We use the signal of the fundamental cavity mode to measure the sample extinction from the change in the cavity line width. To obtain a low-noise dispersion signal of the sample, we exploit the differential frequency shift of the three second order higher modes, TEM_{02}, TEM_{11}, and TEM_{20}. These modes acquire different frequency shifts from a nanoparticle due to the different spatial transverse field distributions, as illustrated in Figure 1b; for example, a particle located in the center shifts the TEM_{02} and TEM_{20} modes that have a local field maximum there, while the cloverleaf-shaped TEM_{11} mode has a field node and thus remains unaffected and serves as a reference line. For our analysis, we consider the frequency difference

$$\Delta\nu = (\Delta\nu_{11} - \Delta\nu_{02}) + (\Delta\nu_{11} - \Delta\nu_{20}) \quad (3)$$

$$= \frac{c\mathfrak{R}(\alpha)}{2\epsilon_0\lambda V_m}[2u_{11}^2 - u_{20}^2 - u_{02}^2] \quad (4)$$

yielding a bloom-shaped pointspread function.

Because of a small ellipticity of the fiber mirror profile, the degeneracy of the TEM_{02}, TEM_{11}, and TEM_{20} modes is lifted,[37] and due to higher-order deviations of the surface profile, the frequency separation between the three modes is not equal and depends on the longitudinal mode order. Figure 2c shows the observed spacing for the particular fiber used for the measurements presented in this work in dependence of the longitudinal mode order q. We find that the spacings between the three modes are nearly equal around 46.5 GHz for the longitudinal mode order $q = 21$; thus, we take all subsequent data at that order. It corresponds to an cavity length of $d = q\lambda/2 = 8.19$ μm, including in particular the penetration of the electric field into the dielectric mirrors.

If the cavity resonance is modulated rapidly, then the time between the occurrence of the three resonances is short, and only disturbances at high frequencies with small amplitudes can affect their frequency difference. We have observed, however, that a too fast modulation itself creates disturbing high frequency noise, while a slower modulation increases the temporal separation of the resonances such that more frequency components disturb the signal. To minimize the time separation of the resonances without increasing the modulation speed, we modulate the phase of the probe laser such that sidebands can be used to probe neighboring resonances at an arbitrarily short time delay. Figure 2a,b shows the modulated cavity transmission signal.

We modulate with a frequency of 23.5 GHz such that the second-order sidebands of neighboring modes come close, as indicated by the gray areas in Figure 2b. For the purpose of data evaluation, the modulation strength is chosen to suppress the carrier and to have a large second-order sideband. The resulting temporal spacing is small enough to be immune against mechanical noise. To quantify the frequency difference, we use an additional phase modulation at a frequency of 1.747 GHz to imprint sidebands that are used as a frequency ruler, as shown in Figure 2d. The frequency splitting between two subsequent transverse modes is determined by fitting six Lorentzians to the signal. Furthermore, the multiple copies of resonances are used to improve signal statistics, especially for the extinction measurements. Note that, due to fiber damage, the measurements in the experiment have been done with a different fiber mirror than the measurements shown Figure 2a,b,d, which illustrate the measurement principle. The latter fiber has a much higher ellipticity and thus a higher mode splitting of 150 GHz, thus, requiring a higher sideband spacing of 37 GHz.

■ BACKGROUND SUBTRACTION

To obtain the sample extinction, we measure the cavity linewidth for the fundamental mode using similar sidebands on many points on the plane mirror that is boustrophedonically raster scanned with a step size of 200 nm at a measurement speed of around 0.25 s/pixel, mainly limited by the online data processing.

In general, the resulting signal of sampling a sparse distribution of particles absorbing or dispersing light with almost 2 orders of magnitude larger resonator modes is a convolution of the sample and the intensity distribution. Due to the very different sizes of the cavity modes and the particles,
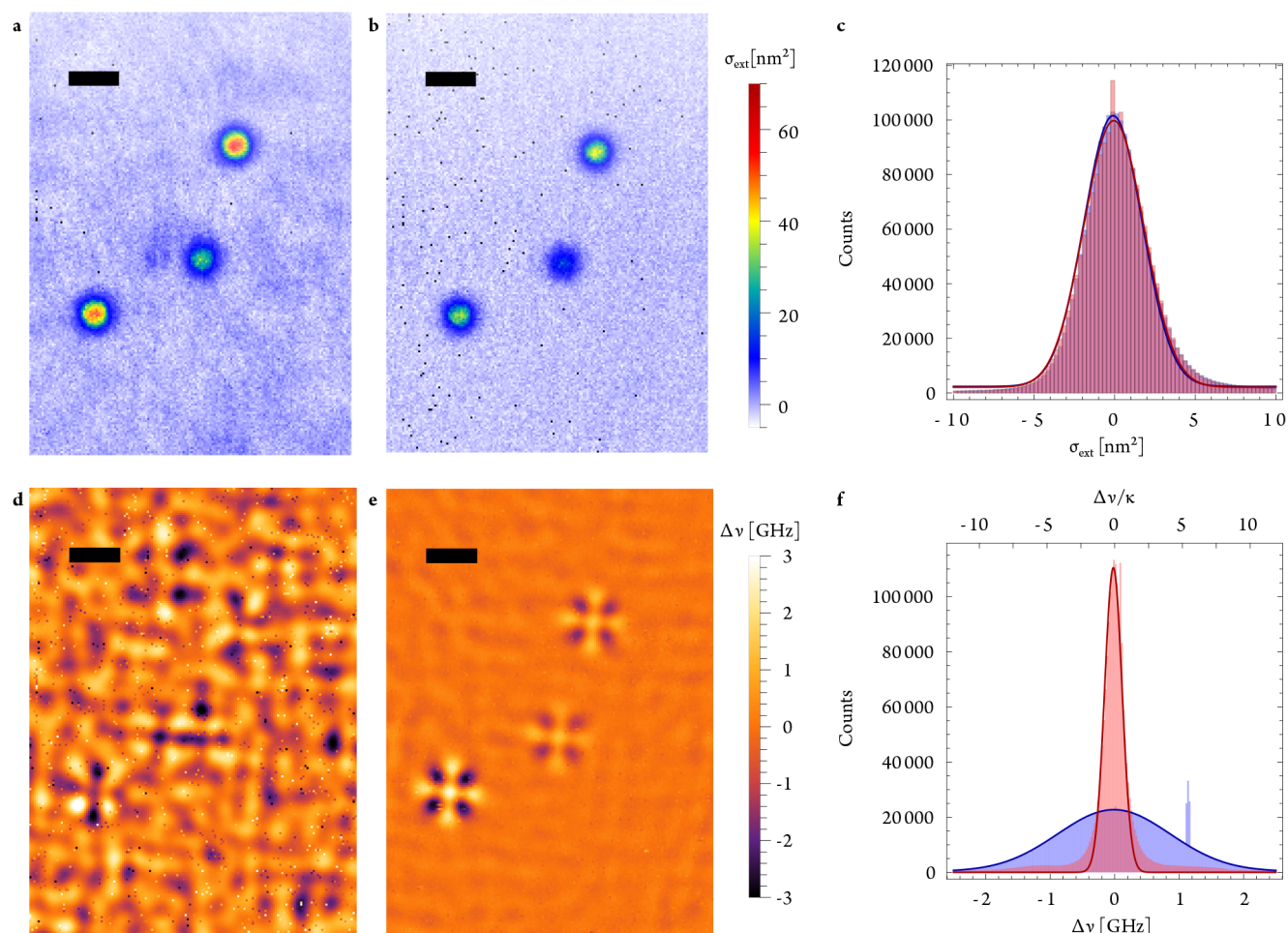
Figure 3. (a) SCM measurement of the extinction cross section of individual gold nanospheres before and (b) after background subtraction. (c) Statistical evaluation of the cavity transmission signal before (blue) and after (red) background subtraction. (d) SCM measurement of the relative frequency shift before and (e) after background subtraction. A large background variation is visible that can be significantly suppressed by a differential measurement. For the corrected picture, faulty pixels have been replaced by the mean value of the surrounding ones. (f) Statistical evaluation of the frequency shift signal before (blue) and after (red) background subtraction. Scale bars 5 μm.

the point spread functions are determined by the resonator modes, while the particle size and properties set the maximum amplitudes. An example of a spatial extinction map is shown in Figure 3a. A corresponding map for the frequency difference signal is shown in Figure 3d. The left figures show the signal for a single measurement, and we observe a significant background variation in particular for the frequency shift signal. We have analyzed the origin of this background in detail and found that it originates from spatial modulation of transverse-mode mixing due to the local variation of the planar mirror, in particular, its local curvature, surface gradient, and nanoscale roughness, see ref 38 for more details.

Here we show that one can suppress this background variation by an additional differential method: we perform measurements before and after application of the nanoparticles at the same location on the mirror and subtract the two measurements. The right panels (Figure 3b,e) show the resulting difference maps. One can see that the background variations get efficiently suppressed, and even high spatial frequencies can be removed due to precise overlapping of the measured areas with the help of markers imprinted to the plane mirror and subsequently by algorithmic image alignment. The remaining noise shows nearly no spatial structure. To quantify

the improvement of the differential technique and the achievable noise limit, we plot all data as a histogram and fit it with a Gaussian profile. Figure 3c and f show corresponding histograms and fits for the extinction cross section and the frequency difference, respectively. We find that the noise in the extinction contrast varies only marginally from a standard deviation of $\Delta\sigma_{ext} = 1.80$ nm^2, with a background to 1.85 nm^2 with subtracted background, despite the visible improvement. This shows that other measurement noise is dominating for this signal. Comparing to a gold nanoparticle probed on the plasmon resonance, this noise level would allow the detection of a particle with a 5 nm diameter. On the other hand, the frequency shift noise reduces by a factor of 6.5, and the remaining noise amounts to $\Delta(\Delta\nu) = 135$ MHz or 0.6 cavity line widths. This corresponds to a minimal detectable polarizability volume of $\alpha_V = \Re(\alpha)/\epsilon_0 = 28000$ nm^3. For comparison, the expected peak frequency shift for a 50 nm GNP probed at 780 nm amounts to 3.5 GHz. In the background-subtracted signal, the characteristic bloom-shaped point spread function becomes clearly visible and can be quantitatively evaluated.

QUANTITATIVE POLARIZABILITY DETERMINATION

We have performed background corrected measurements on a large area of the mirror, 300 μm × 300 μm, and analyzed the peak extinction cross section and the polarizability for 43 GNPs. Figure 3 shows an example area with three isolated GNPs of slightly different sizes.

The extinction cross section of each particle is determined by fitting a Gaussian ($\sigma(x,y) = \sigma_{ext} \exp(-2(x - x_c)^2/w_0^2 - 2(y - y_c)^2/w_0^2)$) to each point spread function. To do so, the coordinates of the particles center (x_c, y_c) are determined using image processing and a particle detection algorithm.[26] To select individual particles, only those with a point spread function having a $1/e^2$ radius of (2 ± 0.3) μm close to the expected mode waist of the cavity ($w_0 = (2 \pm 0.15)$ μm) are considered, which excludes, for example, multiple particles located at small separation. The resulting distribution of extinction cross sections is shown in Figure 4a.

Similarly, we fit the frequency shift signal using the function given in eq 4, which we center on the Gaussian profile of the simulta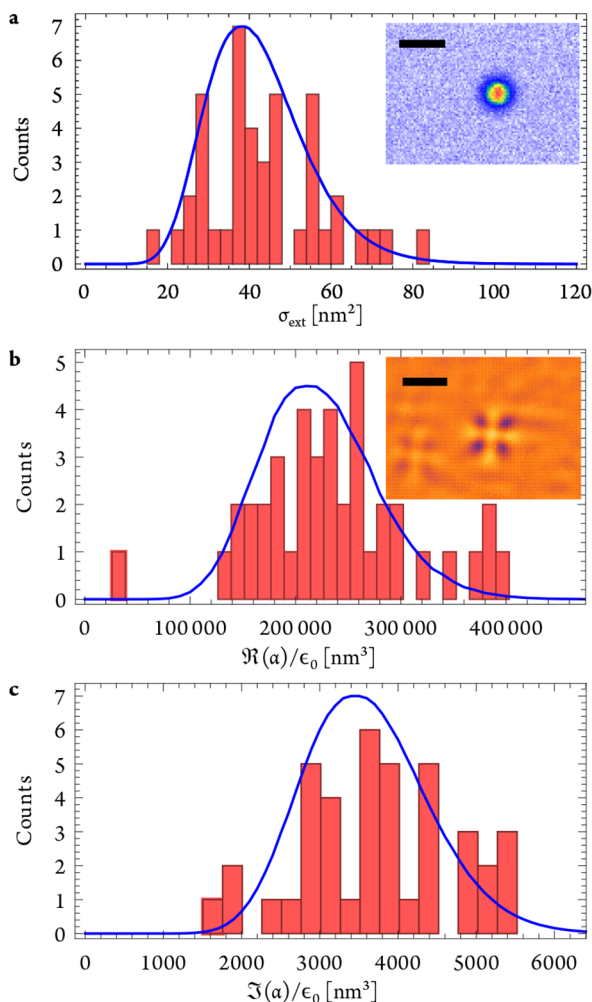neously measured extinction signal. As can be seen from the eq 4, this directly yields the real part of the polarizability of the respective particle, and Figure 4b shows a histogram of the measured polarizabilities.

Knowing the real part of α and the extinction cross section, we can furthermore extract the imaginary part of α via eq 1 and thereby fully determine the complex polarizability. Figure 4c shows the corresponding distribution for $\Im(\alpha)$.

To compare our measurements, we calculate expected distributions of the polarizability as well as the extinction cross section for the particle size distribution specified by the manufacturer. Starting with parameters for the bulk material,[39] we consider effects of the small particle size on the dielectric function[40] to calculate the polarizability of a small sphere far off the plasmon resonance on a dielectric surface[41,42] (see Supporting Information, note 2, for further details).

The measured and calculated probability distributions match very well. The close agreements underline the quantitative nature of our method. This is related to the precise knowledge of the intrinsic losses of the empty cavity, the controlled placement of the particles in the standing wave cavity field, and the precise calibration of the measured frequency shifts.

To estimate the reproducibility, we have measured the extinction cross section of one particle 15 times and obtained a relative standard deviation of 0.5%, giving an estimate for the precision of the measurement (see Supporting Information, note 3, for further details). In a second step, we have measured the extinction cross section of the same particle for subsequent longitudinal mode orders and repeated this experiment five times. This yields a larger variation of 5%, originating from transverse mode mixing effects,[38,43] which is the dominating systematic uncertainty in our measurements and limits the accuracy of the method.

CONCLUSION

In conclusion, we have shown that scanning cavity microscopy can be employed to quantify the complex polarizability of individual nanoparticles with ultrahigh sensitivity and excellent reproducibility. Quantitative values can be deduced by relying only on a few quantities that can be determined precisely: the empty cavity finesse, the cavity line width, and frequency, which all rely only on frequency measurements, and the mode waist, which is directly accessible from the measured maps. This minimizes systematic uncertainties, which we find to be dominated by transverse mode mixing.[38] Notably, the demonstrated differential method does not rely on active stabilization of the cavity and is compatible with significant mechanical noise. Already in the present setting, we achieve a detection noise limit that is sufficient to study a large range of nanomaterials, opening the way for the optical characterization of novel nanomaterials or biologically relevant macromolecules. We note that by using the polarization modes of the cavity, it is straightforward to extend the method to anisotropic materials which show a tensorial polarizability such as ellipsoidally shaped nanoparticles.[26] With a suitably tunable narrow-band laser, the technique can also be extended to spectrally resolved measurements.[28,44] Further improvements can be expected when using a mechanical cavity setup with improved passive stability. We have recently demonstrated a monolithic three-axis scanning cavity setup[45] that improves the passive stability by up to 1000-fold, such that the method described here could be operated also without the need for high-frequency phase modulation. With this, scanning cavity

Figure 4. Measurement results of individual gold nanospheres (histograms) in comparison to calculated distributions (solid lines) of (a) the extinction cross section, (b) the real part of α, and (c) the imaginary part of α calculated from the first two measurements. Scale bars 5 μm; color bars of the insets are the same as in Figure 3.

microscopy could become a powerful tool for the quantitative characterization of nanomaterials.

ASSOCIATED CONTENT

Supporting Information

The Supporting Information is available free of charge at https://pubs.acs.org/doi/10.1021/acsphotonics.1c01131.

> Extinction cross section and cavity losses; Optical properties of metal nanoparticles in the Rayleigh limit; Repeatability of extinction measurements based on scanning cavity microscopy (PDF)

AUTHOR INFORMATION

Corresponding Authors

Matthias Mader − *Fakultät für Physik, Ludwig-Maximilians-Universität, 80539 München, Germany; Max-Planck-Institut für Quantenoptik, 85748 Garching, Germany;* orcid.org/0000-0002-2459-9367; Email: matthias.mader@physik.uni-muenchen.de

David Hunger − *Physikalisches Institut, Karlsruhe Institute of Technology, 76131 Karlsruhe, Germany; Institute for Quantum Materials and Technologies, Karlsruhe Institute of Technology (KIT), 76344 Eggenstein-Leopoldshafen, Germany;* orcid.org/0000-0001-6156-6145; Email: david.hunger@kit.edu

Authors

Julia Benedikter − *Fakultät für Physik, Ludwig-Maximilians-Universität, 80539 München, Germany*

Lukas Husel − *Fakultät für Physik, Ludwig-Maximilians-Universität, 80539 München, Germany*

Theodor W. Hänsch − *Fakultät für Physik, Ludwig-Maximilians-Universität, 80539 München, Germany; Max-Planck-Institut für Quantenoptik, 85748 Garching, Germany*

Complete contact information is available at:
https://pubs.acs.org/10.1021/acsphotonics.1c01131

Notes

The authors declare no competing financial interest.

ACKNOWLEDGMENTS

REFERENCES

(1) Nikolaidou, K.; Sarang, S.; Ghosh, S. Nanostructured photovoltaics. *Nano Futures* **2019**, *3*, 012002.

(2) Gómez-Hens, A.; Fernández-Romero, J.; Aguilar-Caballos, M. Nanostructures as analytical tools in bioassays. *TrAC Trends in Analytical Chemistry* **2008**, *27*, 394−406.

(3) Song, M.; Wang, D.; Peana, S.; Choudhury, S.; Nyga, P.; Kudyshev, Z. A.; Yu, H.; Boltasseva, A.; Shalaev, V. M.; Kildishev, A. V. Colors with plasmonic nanostructures: A full-spectrum review. *Applied Physics Reviews* **2019**, *6*, 041308.

(4) Quinten, M. *Optical Properties of Nanoparticle Systems*; Wiley VCH Verlag GmbH, 2011.

(5) van de Hulst, H. C. *Light Scattering by Small Particles (Dover Books on Physics)*; Dover Publications, 1981.

(6) Bohren, C. *Absorption and Scattering of Light by Small Particles*; Wiley: New York, 1983.

(7) Arbouet, A.; Christofilos, D.; Del Fatti, N.; Vallée, F.; Huntzinger, J. R.; Arnaud, L.; Billaud, P.; Broyer, M. Direct Measurement of the Single-Metal-Cluster Optical Absorption. *Phys. Rev. Lett.* **2004**, *93*, 127401.

(8) Berciaud, S.; Cognet, L.; Poulin, P.; Weisman, R. B.; Lounis, B. Absorption Spectroscopy of Individual Single-Walled Carbon Nanotubes. *Nano Lett.* **2007**, *7*, 1203−1207.

(9) Taylor, R. W.; Sandoghdar, V. Interferometric Scattering Microscopy: Seeing Single Nanoparticles and Molecules via Rayleigh Scattering. *Nano Lett.* **2019**, *19*, 4827−4835.

(10) Mikhailovsky, A. A.; Petruska, M. A.; Stockman, M. I.; Klimov, V. I. Broadband near-field interference spectroscopy of metal nanoparticles using a femtosecond white-light continuum. *Opt. Lett.* **2003**, *28*, 1686.

(11) Celebrano, M.; Savoini, M.; Biagioni, P.; Zavelani-Rossi, M.; Adam, P.-M.; Duò, L.; Cerullo, G.; Finazzi, M. Retrieving the complex polarizability of single plasmonic nanoresonators. *Phys. Rev. B* **2009**, *80*, 153407.

(12) Crut, A.; Maioli, P.; Del Fatti, N.; Vallée, F. Optical absorption and scattering spectroscopies of single nano-objects. *Chem. Soc. Rev.* **2014**, *43*, 3921−3956.

(13) Husnik, M.; Linden, S.; Diehl, R.; Niegemann, J.; Busch, K.; Wegener, M. Quantitative Experimental Determination of Scattering and Absorption Cross-Section Spectra of Individual Optical Metallic Nanoantennas. *Phys. Rev. Lett.* **2012**, *109*, 233902.

(14) Payne, L. M.; Langbein, W.; Borri, P. Polarization-resolved extinction and scattering cross-sections of individual gold nanoparticles measured by wide-field microscopy on a large ensemble. *Appl. Phys. Lett.* **2013**, *102*, 131107.

(15) Zilli, A.; Langbein, W.; Borri, P. Quantitative Measurement of the Optical Cross Sections of Single Nano-objects by Correlative Transmission and Scattering Microspectroscopy. *ACS Photonics* **2019**, *6*, 2149−2160.

(16) Khadir, S.; Andrén, D.; Chaumet, P. C.; Monneret, S.; Bonod, N.; Käll, M.; Sentenac, A.; Baffou, G. Full optical characterization of single nanoparticles using quantitative phase imaging. *Optica* **2020**, *7*, 243.

(17) Stoller, P.; Jacobsen, V.; Sandoghdar, V. Measurement of the complex dielectric constant of a single gold nanoparticle. *Opt. Lett.* **2006**, *31*, 2474.

(18) Vollmer, F.; Arnold, S. Whispering-gallery-mode biosensing: label-free detection down to single molecules. *Nat. Methods* **2008**, *5*, 591−596.

(19) Vollmer, F.; Yang, L. Review Label-free detection with high-Q microcavities: a review of biosensing mechanisms for integrated devices. *Nanophotonics* **2012**, *1*, 267−291.

(20) Heylman, K. D.; Knapper, K. A.; Goldsmith, R. H. Photothermal Microscopy of Nonluminescent Single Particles Enabled by Optical Microresonators. *J. Phys. Chem. Lett.* **2014**, *5*, 1917−1923.

(21) Trupke, M.; Hinds, E. A.; Eriksson, S.; Curtis, E. A.; Moktadir, Z.; Kukharenka, E.; Kraft, M. Microfabricated high-finesse optical cavity with open access and small volume. *Appl. Phys. Lett.* **2005**, *87*, 211106.
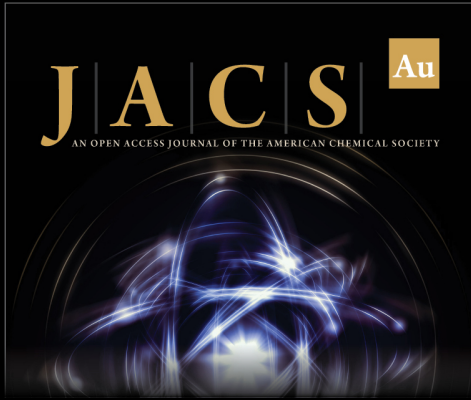
(22) Hunger, D.; Steinmetz, T.; Colombe, Y.; Deutsch, C.; Hänsch, T. W.; Reichel, J. A fiber Fabry-Perot cavity with high finesse. *New J. Phys.* **2010**, *12*, 065038.

(23) Dolan, P. R.; Hughes, G. M.; Grazioso, F.; Patton, B. R.; Smith, J. M. Femtoliter tunable optical cavity arrays. *Opt. Lett.* **2010**, *35*, 3556−3558.

(24) Toninelli, C.; Delley, Y.; Stöferle, T.; Renn, A.; Götzinger, S.; Sandoghdar, V. A scanning microcavity for in situ control of single-molecule emission. *Appl. Phys. Lett.* **2010**, *97*, 021107.

(25) Greuter, L.; Starosielec, S.; Najer, D.; Ludwig, A.; Duempelmann, L.; Rohner, D.; Warburton, R. J. A small mode volume tunable microcavity: Development and characterization. *Appl. Phys. Lett.* **2014**, *105*, 121105.

(26) Mader, M.; Reichel, J.; Hänsch, T. W.; Hunger, D. A scanning cavity microscope. *Nat. Commun.* **2015**, *6*, 7249.

(27) Kelkar, H.; Wang, D.; Martín-Cano, D.; Hoffmann, B.; Christiansen, S.; Götzinger, S.; Sandoghdar, V. Sensing Nanoparticles with a Cantilever-Based Scannable Optical Cavity of Low Finesse and Sub-λ^3-Volume. *Physical Review Applied* **2015**, *4*, 054010.

(28) Hümmer, T.; Noe, J.; Hofmann, M. S.; Hänsch, T. W.; Högele, A.; Hunger, D. Cavity-enhanced Raman microscopy of individual carbon nanotubes. *Nat. Commun.* **2016**, *7*, 12155.

(29) Trichet, A. A. P.; Dolan, P. R.; James, D.; Hughes, G. M.; Vallance, C.; Smith, J. M. Nanoparticle Trapping and Characterization Using Open Microcavities. *Nano Lett.* **2016**, *16*, 6172−6177.

(30) Kohler, L.; Mader, M.; Kern, C.; Wegener, M.; Hunger, D. Tracking Brownian motion in three dimensions and characterization of individual nanoparticles using a fiber-based high-finesse microcavity. *Nat. Commun.* **2021**, *12*, 6385.

(31) Asenbaum, P.; Kuhn, S.; Nimmrichter, S.; Sezer, U.; Arndt, M. Cavity cooling of free silicon nanoparticles in high vacuum. *Nat. Commun.* **2013**, *4*, 2743.

(32) Kimble, H. J. Strong Interactions of Single Atoms and Photons in Cavity QED. *Phys. Scr.* **1998**, *T76*, 127.

(33) Tanji-Suzuki, H.; Leroux, I. D.; Schleier-Smith, M. H.; Cetina, M.; Grier, A. T.; Simon, J.; Vuletić, V. *Advances In Atomic, Molecular, and Optical Physics*; Elsevier, 2011; pp 201−237.

(34) Wickenbrock, A.; Hemmerling, M.; Robb, G. R. M.; Emary, C.; Renzoni, F. Collective strong coupling in multimode cavity QED. *Phys. Rev. A* **2013**, *87*, 043817.

(35) Hunger, D.; Deutsch, C.; Barbour, R. J.; Warburton, R. J.; Reichel, J. Laser micro-fabrication of concave, low-roughness features in silica. *AIP Advances* **2012**, *2*, 012119.

(36) Motsch, M.; Zeppenfeld, M.; Pinkse, P. W. H.; Rempe, G. Cavity-enhanced Rayleigh scattering. *New J. Phys.* **2010**, *12*, 063022.

(37) Uphoff, M.; Brekenfeld, M.; Rempe, G.; Ritter, S. Frequency splitting of polarization eigenmodes in microscopic Fabry-Perot cavities. *New J. Phys.* **2015**, *17*, 013053.

(38) Benedikter, J.; Moosmayer, T.; Mader, M.; Hümmer, T.; Hunger, D. Transverse-mode coupling effects in scanning cavity micrsocopy. *New J. Phys.* **2019**, *21*, 103029.

(39) Johnson, P. B.; Christy, R. W. Optical Constants of the Noble Metals. *Phys. Rev. B* **1972**, *6*, 4370−4379.

(40) Muskens, O. L.; Billaud, P.; Broyer, M.; Del Fatti, N.; Vallee, F. Optical extinction spectrum of a single metal nanoparticle: Quantitative characterization of a particle and of its local environment. *Phys. Rev. B* **2008**, *78*, 205410.

(41) Wind, M. M.; Vlieger, J.; Bedeaux, D. The polarizability of a truncated sphere on a substrate I. *Physica A: Statistical Mechanics and its Applications* **1987**, *141*, 33−57.

(42) Wind, M.; Bobbert, P.; Vlieger, J.; Bedeaux, D. The polarizability of a truncated sphere on a substrate II. *Physica A: Statistical Mechanics and its Applications* **1987**, *143*, 164−182.

(43) Benedikter, J.; Hümmer, T.; Mader, M.; Schlederer, B.; Reichel, J.; Hänsch, T. W.; Hunger, D. Transverse-mode coupling and diffraction loss in tunable Fabry-Pérot microcavities. *New J. Phys.* **2015**, *17*, 053051.

(44) Gebhardt, C.; Förg, M.; Yamaguchi, H.; Bilgin, I.; Mohite, A. D.; Gies, C.; Florian, M.; Hartmann, M.; Hänsch, T. W.; Högele, A.; Hunger, D. Polariton hyperspectral imaging of two-dimensional semiconductor crystals. *Sci. Rep.* **2019**, *9*, 13756.

(45) Casabone, B.; Deshmukh, C.; Liu, S.; Serrano, D.; Ferrier, A.; Hümmer, T.; Goldner, P.; Hunger, D.; de Riedmatten, H. Dynamic control of Purcell enhanced emission of erbium ions in nanoparticles. *Nat. Commun.* **2021**, *12*, 3570.